Journal of Sound and Vibration (1999) **224**(1), 17–32
Article No. jsvi.1997.1301, available online at http://www.idealibrary.com on IDEAL®

MODELLING AND VIBRATION ANALYSIS OF MISALIGNED ROTOR-BALL BEARING SYSTEMS

Y.-S. Lee and C.-W. Lee

Center for Noise and Vibration Control (*NOVIC*), *Department of Mechanical Engineering*, *KAIST*, *Science Town*, *Taejon* 305-701, *South Korea*

(*Received* 15 *April* 1997, *and in final form* 28 *August* 1997)

A dynamic model is derived for misaligned rotor-ball bearing systems driven through a flexible coupling by treating the reaction loads and deformations at the bearing and coupling elements as the misalignment effect. In order to verify the validity of the misaligned rotor system model, experiments are extensively carried out with a laboratory test rig. Both the experimental and simulation results agree well in that, as the angular misalignment increases, the whirling orbits tend to collapse toward a straight line and the natural frequency of the misaligned rotor system associated with the misalignment direction increases largely. It is found that the increase in natural frequency is mostly due to the increase in effective bearing moment stiffness associated with the misalignment direction.

© 1999 Academic Press

1. INTRODUCTION

The vibration in rotating machinery is mostly caused by unbalance, misalignment, mechanical looseness, shaft crack, and other malfunctions. Misalignment is present because of improper machine assembly and thermal distortion of the bearing housing supports, resulting in abnormal rotating preload. However, the perfect alignment between the driving and driven machines cannot be attained [1–3].

In spite of its importance and frequent observations in practice and unlike other malfunctions, only a few researchers have paid attention to misalignment due to the complexity in modelling. In addition, a majority of the recent studies on misalignment have mainly analyzed the effects of coupling misalignment on the vibration of the connected rotor systems: Gibbons [4] and Arumugam *et al*. [5] modelled the reaction forces and moments of misaligned flexible coupling; Sekhar and Prabhu [6] numerically evaluated the effects of coupling misalignment on the $2\times$ vibration response of a rotor-coupling-bearing system; Dewell and Mitchell [7] showed experimentally that the $2\times$ and $4\times$ vibration components are largely dependent upon coupling misalignment; Arumugam *et al*. and Xu and Marangoni [8, 9] showed that the vibration responses due to coupling misalignment mainly occur at the even integer multiples of the rotational speed; Simon [10] evaluated the effect of the coupling misalignment on the bearing vibration, adapting

0022–460X/99/260017 + 16 $30.00/0 © 1999 Academic Press

arithmetically the exciting forces or moments due to the misalignment; Arumugam *et al*. and Sekhar and Prabhu concluded that the effect of misalignment on the critical speed of rotor-bearing-coupling systems is negligible. In the above mentioned previous studies, dominance of even integer multiple harmonics is associated with the shaft rotation or the excitation force transmitted through the misaligned flexible coupling, which is similar to the universal joint effect. They assumed that the bearing stiffnesses are isotropic and the preloads and deformations of the bearing element due to misalignment are absent. However, the preloads generated by misalignment are transmitted through bearings, shaft and coupling, and force the shaft to move into one sector of the bearings. In particular, the preloads at the bearings are known to have significant influence upon the dynamic characteristics such as unbalance response, critical speed and stability of the rotor systems [3, 11, 12]. Hence, to derive an adequate model for the coupling-rotor-bearing systems with misalignment, the effects of misalignment on the preloads and deformations of the bearings as well as the flexible coupling should be included in the modelling.

In this study, a dynamic model for the misaligned rotor system was derived, introducing the reaction loads at the bearing and coupling elements into the model as the misalignment effects. To solve the equation of motion including the non-linear bearing model, we developed a computer program using the Runge–Kutta integration scheme. We also performed experimental studies to investigate the rotor dynamic characteristics related to misalignment and to verify the theoretical development for the misaligned rotor systems.

2. EQUATION OF MOTION

To investigate the effects of misalignment on the rotor dynamic characteristics, we derived a dynamic model for coupling-rotor-ball bearing systems with three types of misalignment as shown in Figure 1: angular, parallel and combined misalignment. In this model, we introduced the reaction forces and moments of bearing and coupling elements as the misalignment effects. Then, we calculated the time responses under misalignment and unbalance force.

2.1. FEM MODEL OF ROTOR SYSTEM

In this study, we utilized the finite element model (FEM) for the flexible shaft and rigid disc elements [13]. Axial vibration, which is known to be an important indication for the presence of misalignment [1–3], is also included in the model. Using the co-ordinates given in Figure 2, the equation of motion for the shaft and disc elements is expressed in partitioned form as

$$\begin{bmatrix} \mathbf{m}^{s+d} & 0 & 0 \\ 0 & \mathbf{m}^{s+d} & 0 \\ 0 & 0 & \mathbf{m}^{a} \end{bmatrix} \begin{Bmatrix} \ddot{\mathbf{y}} \\ \ddot{\mathbf{z}} \\ \ddot{\mathbf{x}} \end{Bmatrix} + \begin{bmatrix} 0 & \mathbf{g}^{s+d} & 0 \\ -\mathbf{g}^{s+d} & 0 & 0 \\ 0 & 0 & 0 \end{bmatrix} \begin{Bmatrix} \dot{\mathbf{y}} \\ \dot{\mathbf{z}} \\ \dot{\mathbf{x}} \end{Bmatrix} + \begin{bmatrix} \mathbf{k}^{s} & 0 & 0 \\ 0 & \mathbf{k}^{s} & 0 \\ 0 & 0 & \mathbf{k}^{a} \end{bmatrix} \begin{Bmatrix} \mathbf{y} \\ \mathbf{z} \\ \mathbf{x} \end{Bmatrix} = \begin{Bmatrix} \mathbf{f}_{y} \\ \mathbf{f}_{z} \\ \mathbf{f}_{x} \end{Bmatrix}, \quad (1)$$

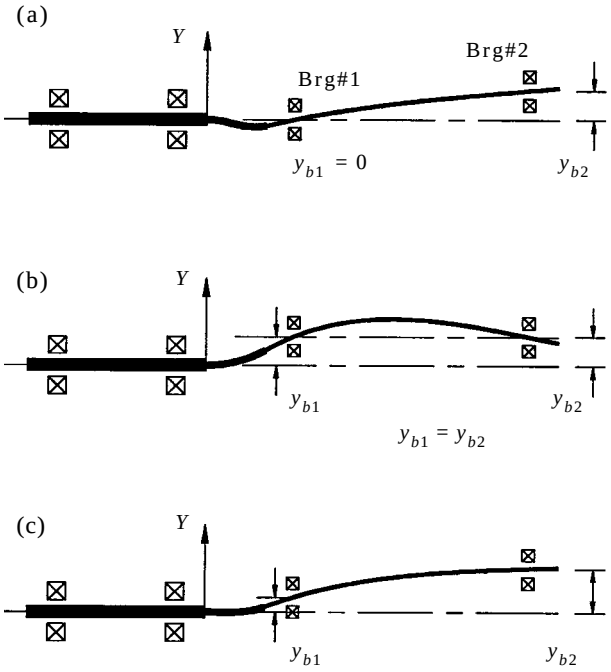

Figure 1. Types of misalignment: (a) angular misalignment; (b) parallel misalignment; (c) combined misalignment.

where

$$\{\mathbf{y}\} = \{q_1 \quad q_2 \quad q_3 \quad q_4\}^T, \quad \{\mathbf{z}\} = \{q_5 \quad q_6 \quad q_7 \quad q_8\}^T,$$
$$\{\mathbf{x}\} = \{q_9 \quad q_{10}\}^T.$$

Here, the superscripts *s* and *d* mean the shaft and disc elements, respectively; the superscript *a* means the axial direction; the matrices, [**m**], [**g**] and [**k**], are the mass, gyroscopic and stiffness matrices, respectively; the force vectors, $\{\mathbf{f}_y\}$ and $\{\mathbf{f}_z\}$,

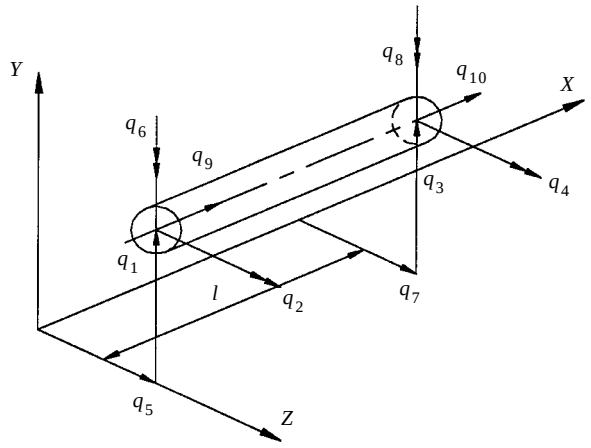

Figure 2. Typical finite rotor element co-ordinates.

include the unbalance, gravity and external forces, and the axial force vector, $\{\mathbf{f}_x\}$, has the axial component of unbalance force and the axial force developed by the axial deformation of the shaft element.

2.2. LOAD AND DEFORMATION OF BALL BEARING

In a rotor system, the ball bearing forms a link between the rotor and the support. If there is a misalignment in the system, the bearing undertakes the radial, axial and moment loads, leading to the deformation of the rolling elements. In the ball bearing with n rolling elements, the bearing reaction forces, F_b's, and moments, M_b's, generated by the bearing deformation can be expressed, using the Hertizian contact stress principle, as [14, 15]

$$F_{bx} = \sum_{j=1}^{n} K_{3/2}\,\delta_j^{3/2} \sin\alpha_j,$$

$$F_{by} = \sum_{j=1}^{n} K_{3/2}\,\delta_j^{3/2} \cos\alpha_j \cos\psi_j,$$

$$F_{bz} = \sum_{j=1}^{n} K_{3/2}\,\delta_j^{3/2} \cos\alpha_j \sin\psi_j, \tag{2}$$

$$M_{by} = \sum_{j=1}^{n} \tfrac{1}{2} D_m K_{3/2}\,\delta_j^{3/2} \sin\alpha_j \sin\psi_j,$$

$$M_{bz} = \sum_{j=1}^{n} \tfrac{1}{2} D_m K_{3/2}\,\delta_j^{3/2} \sin\alpha_j \cos\psi_j$$

Here, δ_j and α_j are the elastic deformation and loaded contact of the j-th rolling element located at angle, ψ_j, from the y-axis; $K_{3/2}$ is the effective stiffness constant for the inner race–rolling element–outer race contacts; and D_m is the pitch diameter of the ball bearing.

2.3. DEFORMED COUPLING ELEMENT

The presence of misalignment between the connected shafts deflects the coupling element and imposes the associated reaction forces and moments on the shafts as shown in Figure 3, although couplings, such as helical and metallic disc couplings, are normally made flexible enough to smooth misalignment. These reaction forces and moments due to misalignment are made up of two parts. One part, which acts on the driving and driven shafts, is due to the transmitted torque. Another part is developed by the deformation of the coupling element [4–6].

First, when there are angular and parallel misalignments in the driven shaft as

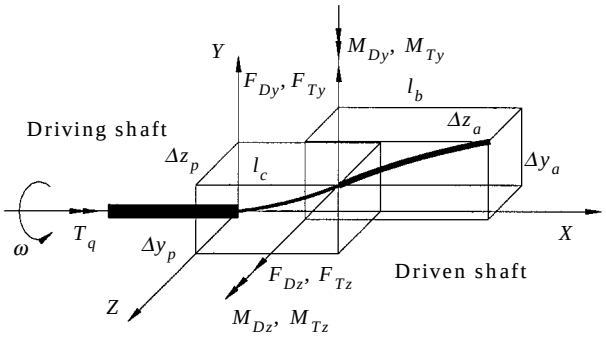

Figure 3. Reaction forces and moments of coupling element.

shown in Figure 3, the moments and forces transmitted to the driven shaft by the driving torque T_q are

$$M_{Ty} = T_q \sin(\phi_a)\cos(\phi_p) + T_q \sin(\phi_p)\cos(\phi_a),$$
$$M_{Tz} = -T_q \sin(\theta_a)\cos(\theta_p) - T_q \sin(\theta_p)\cos(\theta_a), \tag{3}$$
$$F_{Ty} = M_{Tz}/l_c, \qquad F_{Tz} = M_{Ty}/l_c,$$

where

$$\theta_a = \sin^{-1}(\Delta z_a/l_b), \qquad \phi_a = \sin^{-1}(\Delta y_a/l_b), \qquad \theta_p = \sin^{-1}(\Delta z_p/l_c),$$
$$\phi_p = \sin^{-1}(\Delta y_p/l_c),$$
$$\Delta y_a = y_{b2} - y_{b1}, \qquad \Delta z_a = z_{b2} - z_{b1}, \qquad \Delta y_p = y_{b1}, \qquad \Delta z_p = z_{b1}.$$

Here, the subscripts a and p denote the angular and parallel misalignments, respectively; the subscripts y and z denote the y and z directions; θ and ϕ are the bending deflection angles; Δy and Δz are the amounts of misalignment in the y and z directions, respectively; l_c is the distance between the articulating points of the coupling element; l_b is the bearing span; M_T and F_T are the moment and force due to the transmitted torque.

In order to describe the reaction forces and moments generated by the deformation of the coupling element, we modelled the coupling as a beam element with the effective flexural and axial rigidity, EI_c and EA_c, respectively. When the coupling element is deformed due to misalignment, the resulting forces, F_D, and moments, M_D, can be represented as

$$F_{Dy} = \frac{12EI_c}{l_c^3}\left(\Delta y_p - \frac{\phi_a l_c}{2}\right) \qquad F_{Dz} = \frac{12EI_c}{l_c^3}\left(\Delta z_p - \frac{\theta_a l_c}{2}\right),$$

$$M_{Dy} = \frac{6EI_c}{l_c^2}\left(\Delta y_p - \frac{2\phi_a l_c}{3}\right) \qquad M_{Dz} = \frac{6EI_c}{l_c^2}\left(\Delta z_p - \frac{2\theta_a l_c}{3}\right). \tag{4}$$

When the coupling element is deflected by Δx from its free length in the axial direction, the axial force imposed on the connected shafts becomes

$$F_{Dx} = \frac{EA_c}{l_c}\Delta x. \tag{5}$$

2.4. EQUATION OF MOTION

Combining the shaft, bearing and coupling element models, we can obtain the governing equation for a misaligned rotor system as

$$[\mathbf{M}]\{\ddot{\mathbf{Q}}\} + [\mathbf{G} + \mathbf{C}]\{\dot{\mathbf{Q}}\} + [\mathbf{K}]\{\mathbf{Q}\} = \{\mathbf{F}\}_b + \{\mathbf{F}\}_e, \tag{6}$$

where [**M**], [**G**], [**C**] and [**K**] are the mass, gyroscopic, damping and stiffness matrices for the rotor system; the displacement vector, $\{\mathbf{Q}\}$, consists of the bending and axial displacements of the shaft element; $\{\mathbf{F}\}_b$ is the force vector associated with the bearing reaction loads; and the force vector, $\{\mathbf{F}\}_e$, includes the unbalance force, gravity force and coupling reaction forces and moments. In order to describe various misalignment conditions shown in Figure 1, we incorporated the bearing and coupling reaction loads in equation (6) by interconnecting the shaft displacement vector, $\{\mathbf{Q}\}$, with the deformations of the coupling and bearing elements. This interconnection imposes additional reaction loads on the bearing and coupling elements as the misalignment effects. Then equation (6), including the non-linear bearing model, was integrated using the Runge–Kutta integration scheme with a step size of 0·25 ms, in order to obtain the time responses under misalignment and unbalance force.

2.5. ROTOR SYSTEMS

Figure 4 shows the laboratory test rotor system running at the rotational speed, ω. The shaft, which is 10 mm in diameter and 500 mm in length, is supported by two identical deep groove ball bearings described in Table 1, and the rigid disc is located at the mid-span of the shaft. The shaft was modelled as two equal finite element beams with an elastic modulus of $2{\cdot}1 \times 10^{11}$ N/m^2 and density 7800 kg/m^3. The mass, polar and diametrical mass moment of inertia of the disc were 0·26 kg, 0·02 kg m^2 and 0·01 kg m^2, respectively. In the experiments and numerical simulations, the unbalance was set to be 15·7 gmm, and a 30 mm long

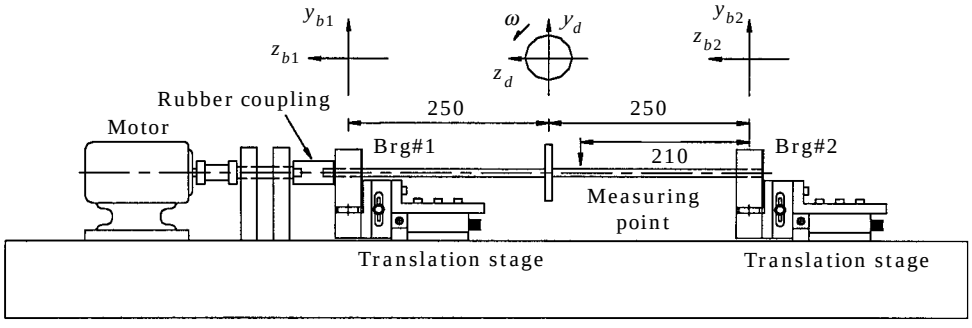

Figure 4. Experimental set-up.

TABLE 1

Specifications for ball bearing

Model	Deep grove ball bearings
Load-deflection constant, $K_{3/2}$	$7{\cdot}566\text{x}10^9$ ($N/m^{3/2}$)
Number of rolling elements, n	8
Radial clearance, e	5 μm
Pitch diameter, D_m	20·5 mm

axisymmetric rubber coupling was used as the coupling element, which was found to be very flexible relative to the shaft. The effective flexural and axial rigidities of the coupling were 0·03 Nm^2 and 728·4 N, respectively. The nominal power and maximum rotational speed of the driving motor were 0·1 hp and 10 000 r.p.m., respectively, and the torque was inversely proportional to the rotational speed. With the experimental set-up, the magnitudes of the bending moments related to the universal joint effect were less than one-hundredth of the bearing reaction moments developed by the angular misalignment. Thus, the universal joint effect in modelling of the misalignment effect was not considered.

The test rig consisted of two translation stages movable by 0·01 mm up to 6·5 mm in the vertical and horizontal directions as shown in Figure 4. The initial shaft alignment was carefully achieved by adjusting the two translational stages so that the fundamental natural frequencies of the rotor system in the y and z directions were equally minimized and the circular whirling orbits were observed in the operating speed range. Using the carefully aligned rotor systems with the two translational stages, various angular and parallel misalignments with less than 0·02 mm positioning error were imposed at the two ball bearing locations. In the experiments, the angular misalignment values, Δy_a and Δz_a, varied from 0 to 2·0 mm for the 500 mm long shaft, whereas the parallel misalignment values, Δy_p and Δz_p, varied from 0 to 1·0 mm for the 30 mm long coupling element.

3. ANALYSIS

In this section, the theoretical model for misaligned rotor systems is experimentally verified, and the effect of misalignment on the dynamic characteristics such as the whirling orbits, frequency responses and parameter sensitivity are extensively investigated.

3.1. ORBIT ANALYSIS

Figure 5 shows the change in whirling orbits measured at the mid-span, as the angular misalignment is varied. The rotor could not be run in the speed range near the critical speed of about 3000 r.p.m., due to excessive vibrations. As mentioned before, the orbits of the initially well-aligned rotor show nearly circular motions in the operating speed range, as shown in Figure 5(a). However, for the angular misalignment along the z direction, as in Figure 5(b and c), the orbits tend to collapse toward an ellipse with the major axis along the $y(z)$ direction for the speed below (above) the critical speed. Likewise, for the angular misalignment along the

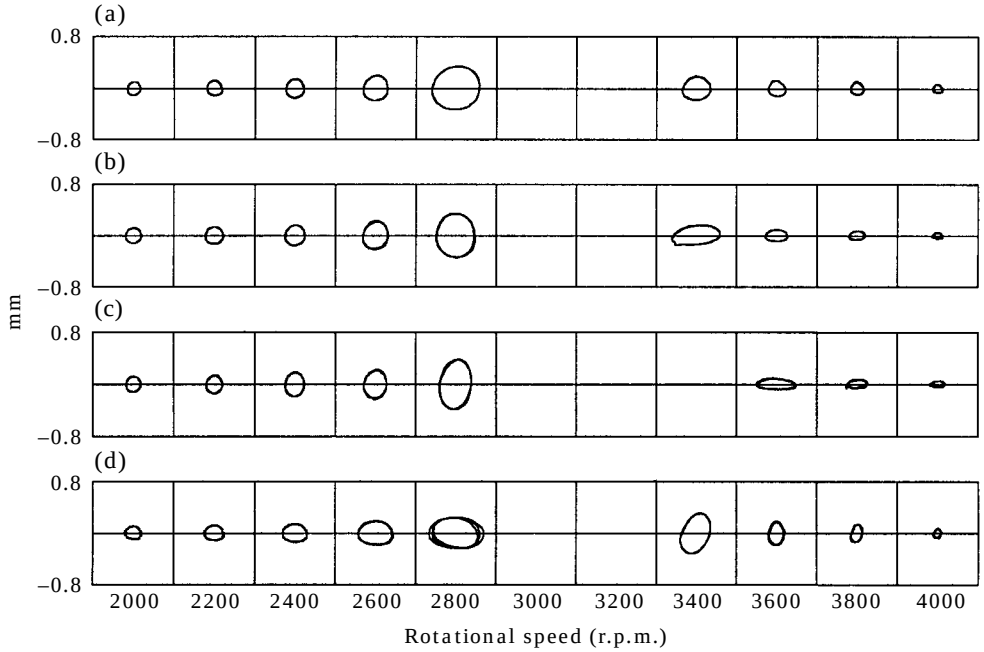

Figure 5. Whirling orbits for angular misalignment: experiment (a) no misalignment; (b) $\Delta z_a = 1{\cdot}0$ mm: (c) $\Delta z_a = 2{\cdot}0$ mm; (d) $\Delta y_a = 2{\cdot}0$ mm.

y direction, as in Figure 5(d), as the rotor passes through the critical speed, the major axis of the elliptic whirling orbit is changed from the z direction to the y direction. The angle of inclination made by the major axis of the elliptic orbit with the y-axis [16] is well represented in Figure 6. Note that the angle of inclination is perpendicular to the angular misalignment direction below the critical speed and it coincides with the misalignment direction above the critical speed. Figure 7 shows the simulated whirling orbits for the same misalignment conditions as in Figure 5. The comparison between the results in Figures 5 and 7 clearly indicates that the simulation results represent well the elliptic whirling motions observed

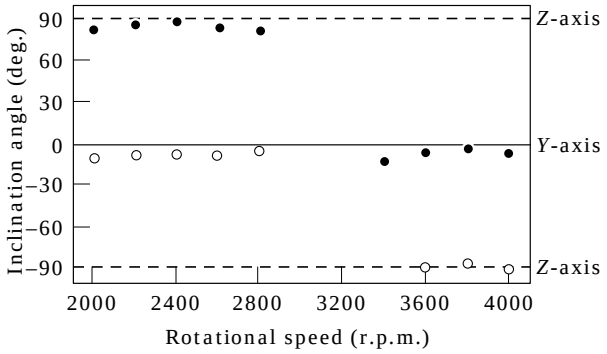

Figure 6. Inclination angle for the synchronous component of whirling orbit. ○, $\Delta z_a = 2{\cdot}0$ mm; ●, $\Delta y_a = 2{\cdot}0$ mm.

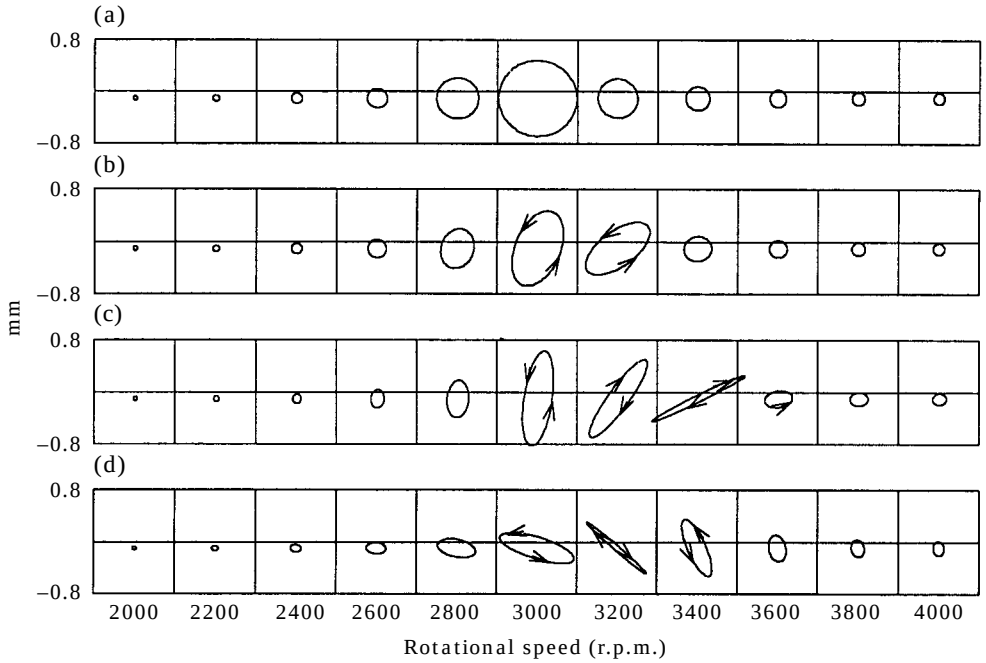

Figure 7. Whirling orbits for angular misalignment: simulation (a) no misalignment; (b) $\Delta z_a = 1{\cdot}0$ mm; (c) $\Delta z_a = 2{\cdot}0$ mm; (d) $\Delta y_a = 2{\cdot}0$ mm.

from the experiments, and the minor (major) axes of the elliptic whirling orbits below (above) the critical speed give the angular misalignment direction. The simulation results in Figure 7 confirm that, as the angular misalignment increases, the anisotropic nature in bearing stiffness also increases so that the backward whirling motions are likely to occur near the critical speed of the well-aligned rotor. The elliptic whirling motion, which is found to be a typical vibration characteristic of misalignment, is due to the fact that more resistance to motion is induced in the misalignment direction than in the well-aligned direction so that the rotor feels a higher effective bearing stiffness in that direction.

Figures 8 and 9 show the whirling orbits for parallel misalignment. Unlike the angular misalignment, the whirling orbits tend to remain unchanged, although the parallel misalignment increases. This is mainly because the coupling element is very flexible relative to the connected shafts, and thus the coupling reaction forces and the moments due to the parallel misalignment are negligibly small, compared with the bearing reaction loads developed by the angular misalignment. This leads to an insignificant influence on the whirling orbit and the bearing stiffness referred to in section 3.2.

3.2. EFFECTIVE BEARING STIFFNESS

To further investigate the aforementioned phenomenon associated with the increase in bearing stiffness along the angular misalignment direction, we

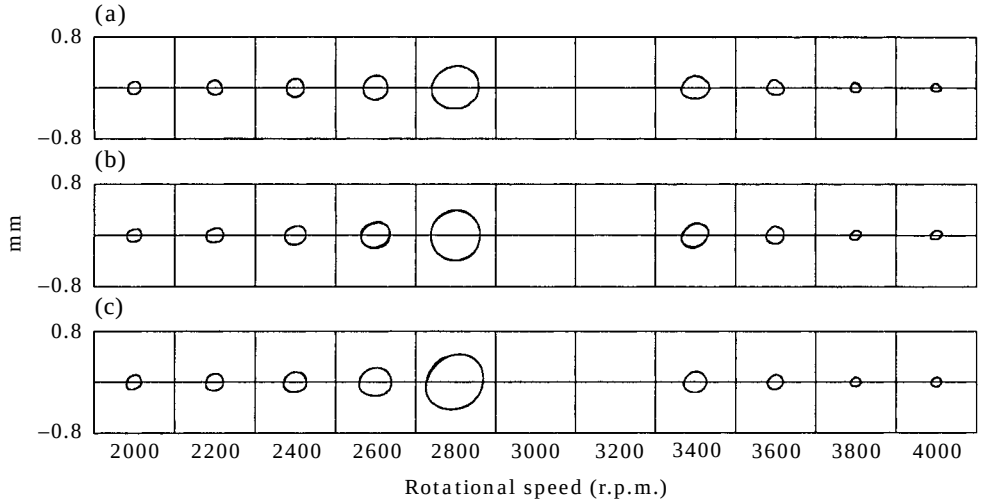

Figure 8. Whirling orbits for parallel misalignment: experiment (a) no misalignment; (b) $\Delta y_p = 0{\cdot}5$ mm; (c) $\Delta y_p = 1{\cdot}0$ mm.

theoretically calculated the effective linear and moment bearing stiffness [15], using the relationships between the bearing loads and deformations in equation (2), i.e.,

$$k_{bij} = \frac{\partial F_i}{\partial \delta_j}; \quad i, j = x_b, y_b, z_b, \theta_{by}, \theta_{bz}, \tag{7}$$

where F_i is the i-th component of the bearing reaction force and moment, and x_b, y_b, z_b, θ_{by} and θ_{bz} are the bearing displacements. For convenience, we then defined the effective mean bearing stiffness matrix, $[\mathbf{K}]_b$, consisting of the effective mean bearing stiffnesses calculated at an arbitrarily chosen low rotational speed

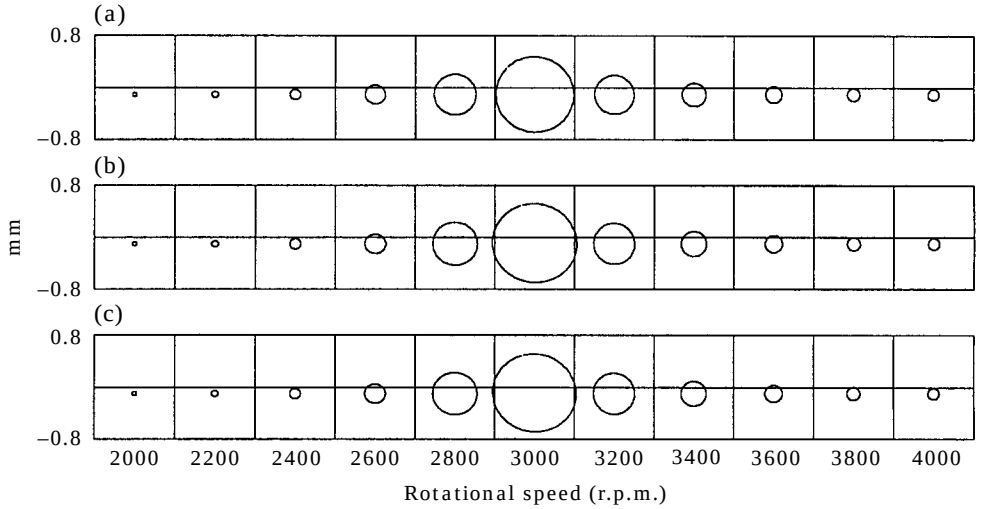

Figure 9. Whirling orbits for parallel misalignment: simulation (a) no misalignment; (b) $\Delta y_p = 0{\cdot}5$ mm; (c) $\Delta y_p = 1{\cdot}0$ mm.

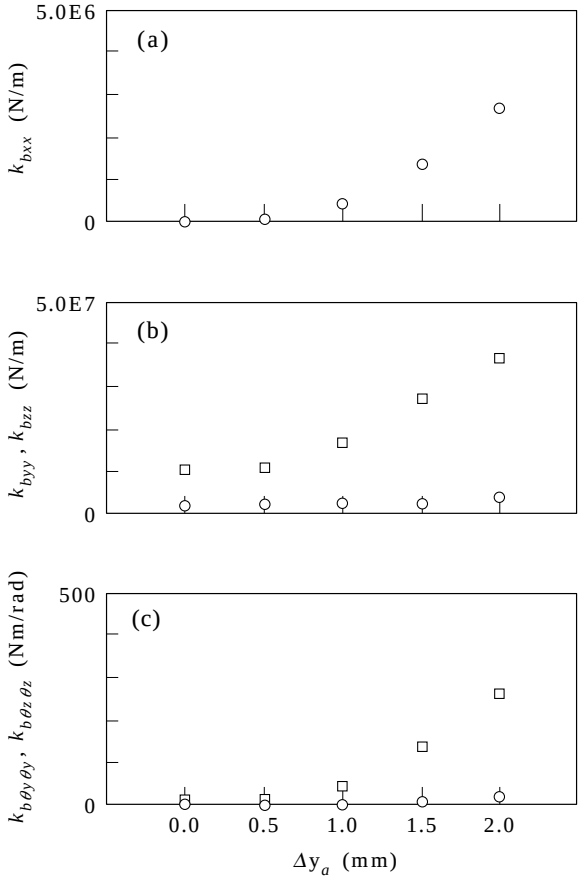

Figure 10. Effective mean bearing stiffnesses for y-directional angular misalignment at Brg # 2. (a) k_{bxx} ; (b) k_{byy} (□) k_{bzz} (○); (c) $k_{b\theta y\theta y}$ (○), $k_{b\theta z\theta z}$ (□).

of 200 r.p.m. Figures 10 and 11 show the calculated effective mean bearing stiffnesses for the $y(z)$-directional angular misalignment at Brg # 2, as the angular misalignment changes. Note that the difference in k_{byy} and k_{bzz} for the y and z directional angular misalignment is mainly due to gravity effect. For the y-directional angular misalignment, the gravity effect decreases (increases) the reaction force due to the shaft bending on Brg # 1(Brg # 2) and thus the effective bearing stiffness, k_{byy}, in Brg # 1(Brg # 2), due to the hardening effect of the rolling elements. On the other hand, the effective bearing stiffnesses, k_{bzz}, for the z-directional angular misalignment are free of gravity. As a result, there is a difference between k_{byy} and k_{bzz}. The mean bearing stiffness, k_{byy} and $k_{b\theta_z\theta_z}$ (k_{bzz} and $k_{b\theta_y\theta_y}$), for the misalignment in the y (z) direction increase largely relative to other bearing stiffnesses, since the increase in the effective bearing linear and moment stiffnesses occurs in association with the misalignment direction. This is the major cause of elliptic whirling motions of the angular misaligned rotor system.

3.3. FREQUENCY RESPONSE FUNCTION

In order to investigate the effects of misalignment on the natural frequency of the misaligned rotor system, we defined the frequency response between the

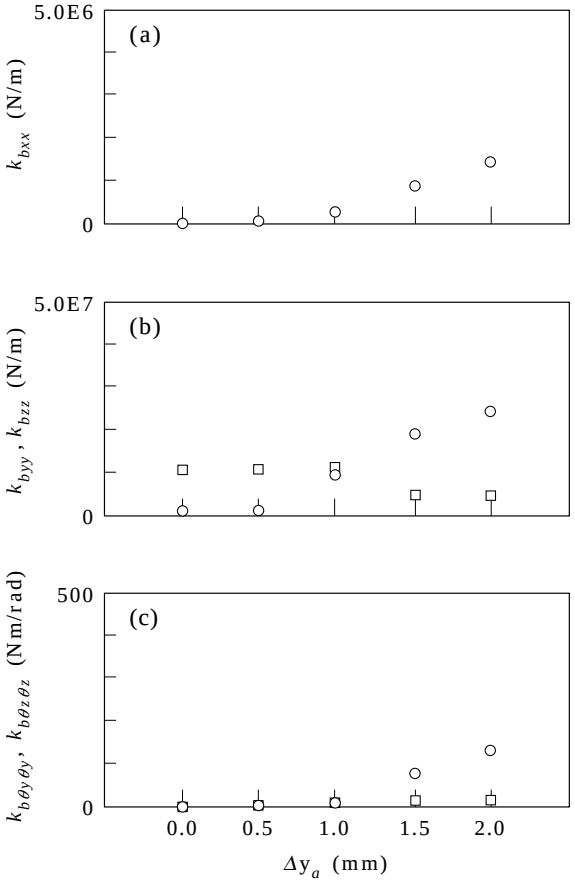

Figure 11. Effective mean bearing stiffnesses for z-directional angular misalignment at Brg # 2. (a) k_{bxx} ; (b) k_{byy} (□) k_{bzz} (○); (c) $k_{b\theta y\theta y}$ (○), $k_{b\theta z\theta z}$ (□).

excitation and response at the disc location, introducing the effective mean bearing stiffness matrix defined in the previous section. The linear governing equation for the misaligned rotor system can then be expressed as

$$[\mathbf{M}]\{\ddot{\mathbf{Q}}\} + [\mathbf{G} + \mathbf{C}]\{\dot{\mathbf{Q}}\} + [\mathbf{K} + \mathbf{K}_b]\{\mathbf{Q}\} = \{\mathbf{F}\}_e, \tag{8}$$

since the bearing force is defined as

$$\{\mathbf{F}\}_b = -[\mathbf{K}]_b \{\mathbf{Q}\}. \tag{9}$$

From equation (8), we can readily derive the frequency response between $\{\mathbf{F}\}_e$ and $\{\mathbf{Q}\}$. Figure 12 shows the typical measured frequency response functions of the test rotor at rest. Note that, as misalignment is absent, the fundamental natural frequencies, in the y and z directions, of the rotor system are 50·1 and 49·6 Hz, respectively. As the angular misalignment increases, the y-directional natural frequency is increased significantly as shown in Figure 12(a). On the other hand, the natural frequencies remained almost unchanged for the parallel misalignment as shown in Figure 12(b). The change in natural frequency for the angular and

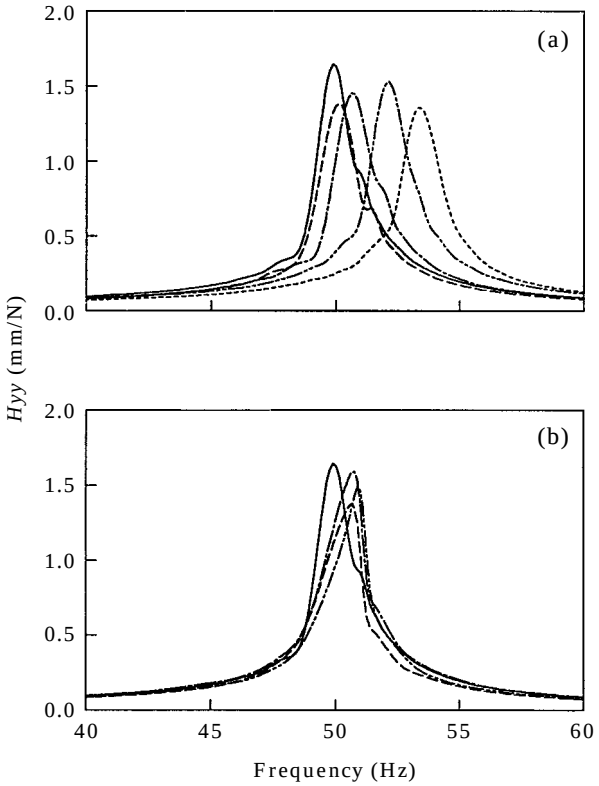

Figure 12. Frequency response function: experiment (a) angular misalignment:—, $\Delta y_a = 0{\cdot}0$; – – –, $\Delta y_a = 0{\cdot}5$; –·–, $\Delta y_a = 1{\cdot}0$; –··–, $\Delta y_a = 1{\cdot}5$; ····, $\Delta y_a = 2{\cdot}0$; (b) parellel misalignment: —, $\Delta y_p = 0{\cdot}0$; – – –, $\Delta y_p = 0{\cdot}5$; –·–, $\Delta y_p = 0{\cdot}8$; –··–, $\Delta y_p = 1{\cdot}0$.

parallel misalignments is summarized in Table 2, where the experimental and simulation results were taken from the rotor systems at rest. Note that the $y(z)$-directional angular misalignment tends to largely increase the $y(z)$-directional natural frequency, ω_{ny} (ω_{nz}), due to the large increase in bearing stiffnesses, k_{byy} and $k_{b\theta_z\theta_z}$ (k_{bzz} and $k_{b\theta_y\theta_y}$), as cited in the previous section. Also, the small increase in the natural frequency, ω_{nz} (ω_{ny}), is due to the small cross-effect of the ball bearing. As a result, the natural frequencies in the y and z directions are separated. The unbalance responses are largely increased near two critical speeds, and the backward whirling motions are generated between the critical speeds, as shown in Figures 7(c and d). However, for the parallel misalignment as given in Table 2(c), the natural frequencies are nearly unchanged, mainly because the coupling element in use is very flexible in bending.

3.4. SENSITIVITY ANALYSIS

As mentioned above, the angular misalignment increases the natural frequency associated with the misalignment direction, due to the increase in the effective bearing stiffness. In order to identify which stiffness most affects the natural frequency of the misaligned rotor systems, we performed the sensitivity analysis using Taguchi's method [17]. Here, we chose the effective bearing linear and

TABLE 2

Fundamental natural frequencies of the misaligned rotor system

	Experiment		Simulation	
	ω_{ny} (Hz)	ω_{nz} (Hz)	ω_{ny} (Hz)	ω_{nz} (Hz)
(a) *y-directional angular misalignment*				
Δy_a (mm):				
0·0	50·1	49·6	49·8	49·4
0·5	50·4	49·6	49·8	49·4
1·0	51·0	49·8	50·6	49·5
1·5	52·4	50·3	52·2	49·6
2·0	53·6	50·8	54·3	49·8
(*b*) *z-directional angular misalignment*				
Δz_a (mm):				
0·0	50·1	49·6	49·8	49·4
0·5	50·3	49·9	49·8	49·4
1·0	50·3	50·9	49·9	50·1
1·5	50·6	52·3	50·1	51·8
2·0	51·3	53·6	50·4	54·2
2·5	51·6	55·4	50·8	57·3
(*c*) *y-directional parallel misalignment*				
Δy_p (mm):				
0·0	50·1	49·6	49·8	49·4
0·5	50·6	49·6	49·8	49·4
0·8	50·7	49·5	49·8	49·4
1·0	50·9	49·5	49·8	49·4

moment stiffnesses as the control factors and the natural frequency associated with the misaligned direction as the performance index (response) for each three-level experiment combination. The three levels for each factor were set to the values corresponding to $-10\,\%$, 0, and $+10\,\%$ of the corresponding effective mean bearing stiffness. Figure 13 shows that the moment stiffness associated with the misalignment direction, $k_{b\theta_y\theta_y}$, gives the most significant influence on the natural frequency of the misaligned rotor system, which is followed by the cross coupled bearing stiffness, $k_{by\theta_y}$. Note that the two bearings play an identical role in the sensitivity analysis because the flexible coupling element has little influence on the dynamics.

4. CONCLUSIONS

The theoretical model for the coupling-rotor-ball bearing systems with misalignment was derived, including the loads and deformations of the bearings as well as the flexible coupling as the misalignment effects. Throughout the extensive experimental and simulation works, the validity of the model was successfully verified and the rotor dynamic characteristics related to misalignment were investigated.

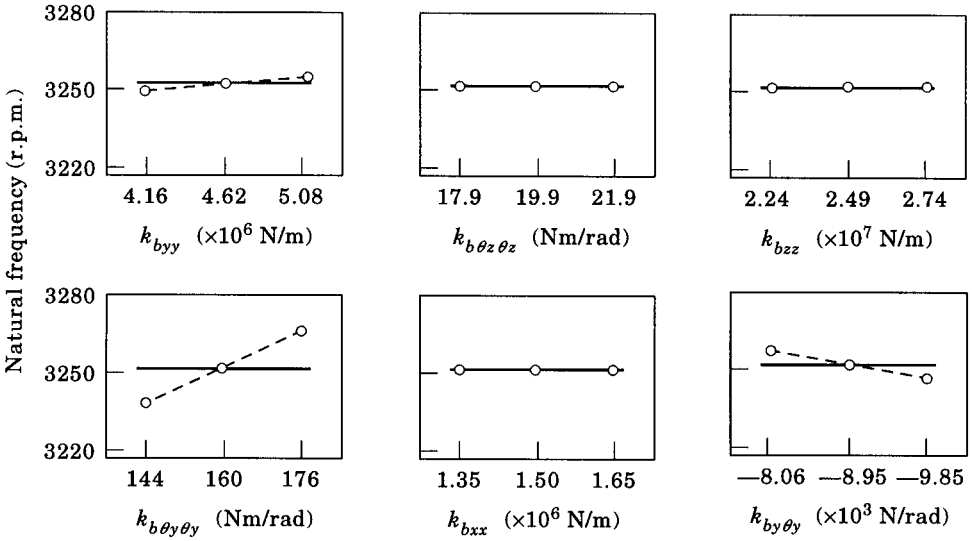

Figure 13. Sensitivity analysis for bearing stiffness using Taguchi method; $\Delta z_a = 2{\cdot}0$ mm.

The experimental and simulation results suggest that the whirling orbits tend to collapse toward a straight line, and the natural frequency associated with the misalignment direction increases largely, as angular misalignment increases, due to the increase in the effective moment stiffness of bearing. On the other hand, for parallel misalignment, the whirling orbit and natural frequency are not changed, when very flexible coupling is used. These phenomena have not been fully reported in the literature where the bearing was normally assumed to be isotropic in stiffness.

REFERENCES

1. M. J. Goodwin 1989 *Dynamics of Rotor-Bearing Systems*. London: Unwin Hyman Ltd.
2. J. M. Vance 1988 *Rotordynamics of Turbomachinery*. New York: John Wiley & Sons.
3. Bently Nevada 1993 *Technical Training*; *Machinery Diagnostics Course*.
4. C. B. Gibbons 1976 *Proceedings of the 5th Turbomachinery Symposium*, *Gas Turbine Laboratories*, *Texas A&M University*, 111–116. Coupling misalignment forces.
5. P. Arumugam, S. Swarnamani and B. S. Prabhu 1995 *ASME Design Engineering Technical Conferences* **84**, 1049–1054. Effects of coupling misalignment on the vibration characteristics of a two stage turbine rotor.
6. A. S. Sekhar and B. S. Prabhu 1995 *Journal of Sound and Vibration* **185**, 655–671. Effects of coupling misalignment on vibrations of rotating machinery.
7. D. L. Dewell and L. D. Mitchell 1984 *ASME Transactions on Journal of Vibration, Acoustics, Stress, and Reliability in Design* **106**, 9–16. Detection of a misaligned disk coupling using spectrum analysis.
8. M. Xu and R. D. Marangoni 1994 *Journal of Sound and Vibration* **176**, 663–679. Vibration analysis of a motor-flexible coupling-rotor system subject to misalignment and unbalance, Part I: theoretical model and analysis.
9. M. Xu and R. D. Marangoni 1994 *Journal of Sound and Vibration* **176**, 681–691. Vibration analysis of a motor-flexible coupling-rotor system subject to misalignment and unbalance, Part II: experimental validation.

10. G. SIMON 1992 *Proceedings of the Institution of Mechanical Engineers, Journal of Mechanical Engineering* **206**, 29–39. Prediction of vibration behaviour of large turbomachinery on elastic foundations due to unbalance and coupling misalignment.
11. T. C. LIM and R. SINGH 1990 *Journal of Sound and Vibration* **139**, 201–225. Vibration transmission through rolling element bearing, Part II: system studies.
12. M. F. WHILE 1979 *ASME Transactions on Journal of Applied Mechanics* **46**, 677–684. Rolling element bearing vibration transfer characteristics: effect of stiffness.
13. Y. D. KIM and C. W. LEE 1986 *Journal of Sound and Vibration* **111**, 441–456. Finite element analysis of rotor-bearing systems using a modal transformation matrix.
14. T. A. HARRIS 1984 *Rolling Bearing Analysis*. New York: John Wiley & Sons.
15. T. C. LIM and R. SINGH 1990 *Journal of Sound and Vibration* **139**, 179–199. Vibration transmission through rolling element bearings, part I: bearing stiffness formulation.
16. C. W. LEE 1993 *Vibration Analysis of Rotors*. Kluwer Academic Publishers.
17. M. S. PHADKE 1989 *Quality Engineering Using Robust Design*. Englewood Cliffs, NJ: Prentice-Hall.